All-PM Divided Pulse Fiber Oscillator Mode-locked with the Optical Kerr-effect

MARVIN EDELMANN,[1,2,3,*] YI HUA,[1,4] GABOR KULCSAR[5] AND FRANZ X. KÄRTNER[1,4]

[1] *Center for Free-Electron Laser Science CFEL, Deutsches Elektronen-Synchrotron DESY, Notkestr. 85, 22607 Hamburg, Germany*
[2] *Department of Physics, Universität Oldenburg, Ammerländer Heerstr. 114-118, 26111 Oldenburg, Germany*
[3] *Cycle GmbH, Notkestr. 85, 22607 Hamburg, Germany*
[4] *Department of Physics, Universität Hamburg, Jungiusstr. 9, 20355 Hamburg, Germany*
[5] *Laser Impulse, Dr. Gabor Kulcsar, Wiesenkamp 30, 24226 Heikendorf, Germany*
**Corresponding author: marvin edelmann@desy.de*

In this letter, we investigate a Yb-doped mode-locked fiber oscillator that uses coherent pulse division and recombination to avoid excessive nonlinear phase shifts. The mode-locking mechanism of the laser is based on the accumulation of a differential nonlinear phase between orthogonal polarization modes in the polarization-maintaining fiber segment. The inserted coherent pulse divider, based on YVO_4-crystals rotated successively by 45°, enables stable and undistorted mode-locked steady-states. The output pulse energy is increased from 89 pJ in the non-divided operation by ~6.5 dB to more than 400 pJ with three divisions. A measurement of amplitude-fluctuations reveals a simultaneous broadband noise suppression of up to ~9 dB in the frequency range from 10 kHz to 2MHz.

Applications for mode-locked fiber oscillators is constantly growing and already includes many scientific fields and state-of-the-art technologies such as frequency metrology [1], seeding high-power amplifiers [2], synchronization and timing distribution [3] and optical microwave generation [4]. Rapid progress in these applications necessitates a continuous improvement of fiber oscillators in terms of environmental stability and output characteristics such as the obtainable pulse energy and noise performance. A key component of ultrafast fiber oscillators is the saturable absorber (SA) which often determines the cavity structure and the achievable output parameters [5-7]. Among the variety of mode-locking mechanisms, *artificial* SAs based on the optical Kerr-effect are promising candidates for many applications once environmentally stable implemented based on polarization-maintaining fibers [8], self-starting operation [9] and superior noise performance [10-12]. A well-established technique utilizes asymmetric fiber loops known as nonlinear amplifying/optical loop mirrors (NALM/NOLM), often in combination with a non-reciprocal phase bias that is required for self-starting operation [13]. In these variations of a Sagnac-interferometer, the self-amplitude modulation has its origin in the accumulation of a nonlinear phase difference between counter-propagating pulses in the fiber loop [14]. More than 20 years earlier, Fermann et. al. proposed an alternative linear cavity structure that allows Kerr-type mode-locking by using co-propagating orthogonal polarization modes in a PM-fiber to accumulate the required nonlinear phase difference with a compensation of linear phase shifts [15]. Despite the advantages of the mentioned Kerr-type mode-locked oscillator structures in all-PM configuration, their performance is still fundamentally limited by the roundtrip nonlinear phase shift and the occurrence of multiple pulse formation due to soliton splitting or wave-breaking if the pulse energy exceeds a certain threshold [16,17]. The achievable intracavity power further restricts the pulse energy and the laser noise performance in terms of phase noise, timing-jitter, and amplitude-fluctuations at the output [18-20]. Different approaches have been proposed to reduce the roundtrip nonlinear phase shift and scale up energy. Besides scaling the fiber core size with the implementation of large-mode area (LMA) fibers [21], it is possible to introduce a large breathing ratio of the pulse duration and thus reduce the nonlinear phase shift per roundtrip by accessing the dissipative or dispersion-managed soliton regime through an engineered all-normal dispersion or a net-dispersion close to zero, respectively [22,23]. In 2014, Lamb et. al. further proposed the application of a coherent divided pulse amplification (DPA) scheme to reduce the pulse peak power in a non-PM, SESAM mode-locked oscillator leading to a significant increase of the output pulse energy [24]. While the concept of DPA is routinely used in amplifier systems nowadays [25,26], there is not yet any information available on the possibility of a stable implementation within an all-PM oscillator cavity with artificial SA. Consequently, in this letter we demonstrate and investigate for the first time the implementation of a coherent division and recombination scheme in such an all-PM cavity structure to increase the obtainable pulse energy and improve the noise performance. The Kerr-type SA mechanism is based on the accumulation of a differential nonlinear phase shift $\Delta\varphi_{nl}$ between orthogonal polarization modes in the PM-fiber segment as proposed in Ref. [15]. The sinusoidal system transmission function $T(\Delta\varphi_{nl})$ in combination with a non-reciprocal phase bias allows for stable and undistorted mode-locking. The implemented pulse divider scheme consists of multiple number of YVO_4- crystals rotated by 45° in conjunction with the birefringent fiber segment [24]. In the experiment, an increase in

output power by up to 6.5 dB is obtained with 3 pulse divisions in comparison with the fundamental mode-locked state with no pulse divisions. Measurements of the RF-spectrum and the intensity-fluctuations reveal a reduced noise-level in the offset-frequency range from 10 kHz to ~2 MHz for an increasing number of divisions.

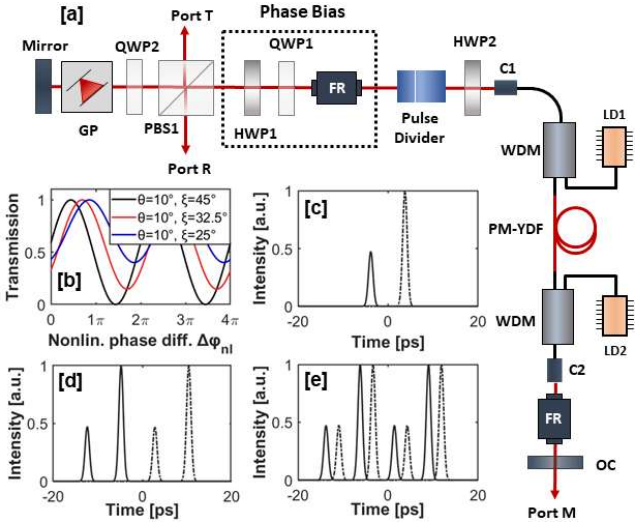

Fig. 1: [a]: Experimental setup of the all-PM divided pulse oscillator. GP: Grating pair, QWP: Quarter-wave plate, PBS: Polarizing beam-splitter, HWP: Half-wave plate, FR: Faraday-rotator, LD: Laser diode, WDM: Wavelength division multiplexer, YDF: Ytterbium-doped fiber, OC: Output coupler, C: fiber collimator. [b]: Transmission function $T(\Delta\varphi_{nl})$ for different rotation angles of HWP1 (θ) and QWP1 (ξ). [c]: Simulated divided pulse train behind the 10 mm YVO_4-crystal (45°-rotation to the transmission axis of PBS1) with one pulse parallel to the slow (solid) and fast axis (dashed) for $\theta = 10°$ and $\xi = 25°$. [d]: Divided pulses after an additional, 45°-rotated, 20 mm YVO_4-crystal in the divider. [e]: Divided pulses at Port M with third division from the PM-fiber segment.

A schematic of the all-PM divided pulse oscillator (DPO) is shown in Fig.1 [a]. The 2.2 m fiber segment contains a 0.6 m highly Yb-doped gain fiber (CorActive Yb-401 PM) that is bi-directionally pumped by two 0.9 W laser diodes at 976 nm (Thorlabs BL976-PAG900), coupled into the fiber with wavelength-division multiplexers (WDM). In the free-space arm on the C2 collimator side, the light is transmitted through a 45°-Faraday-rotator (FR, single-pass) and is subsequently partially reflected the cavity end by an output coupler (OC, 15% transmission) that enables the analysis of the divided pulse bursts through the monitor Port M. The fiber output at collimator C1 is followed by the second free-space arm containing a YVO4-based pulse divider and the non-reciprocal phase bias that consists of a 45°-FR, a quarter-wave plate (QWP1) and a half-wave plate (HWP1). A polarization-insensitive transmission grating pair (LightSmyth T-1000-1040 Series) allows tunable dispersion-management. The laser is mode-locked in the soliton regime with a fixed net dispersion of $\sim -104 \cdot 10^{-3}$ ps^2 and a repetition rate of 36.7 MHz. Soliton mode-locking is chosen for the experiment to ensure pulse durations of <1 ps in the PM-fiber to avoid a time-wise overlap of the divided pulses. In the fundamental state of the oscillator without YVO_4-crystals, the orthogonal polarization modes in the PM-fiber accumulate a nonlinear phase difference $\Delta\varphi_{nl}$ if there is an asymmetric energy splitting ratio ε [27]. In this case, the value of ε together with the shape of the sinusoidal SA transmission function $T(\Delta\varphi_{nl})$ is fully determined by the settings of the waveplate angles θ (HWP1) and ξ (QWP1) in the phase bias as derived e.g., in Ref. [10]. Besides an accumulation of $\Delta\varphi_{nl}$, the PM fiber's birefringence of $B=0.381 \cdot 10^{-3}$ (Coherent PM980-XP) further results in a shift between the polarization modes with ~1.3 ps/m that is compensated with a Faraday-mirror which ensures an identical optical path for both modes through the 90°-rotated back-reflection.

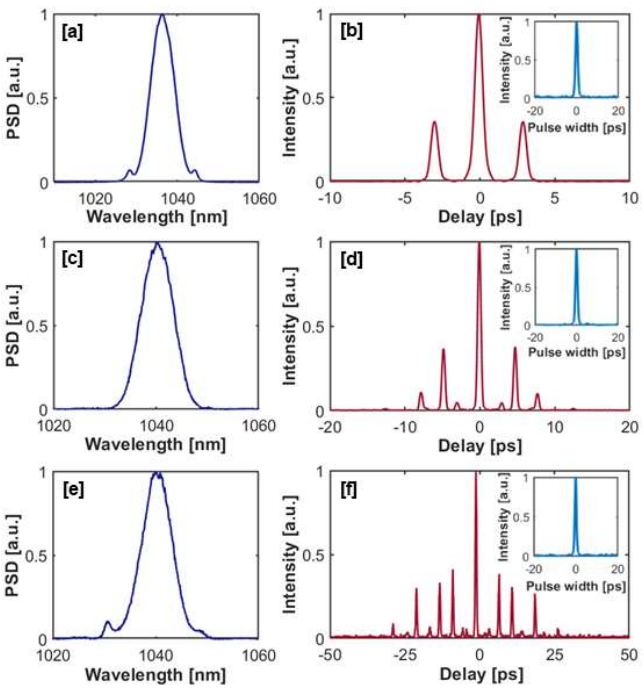

Fig. 2: [a]: Spectral bandwidth at Port T with FWHM of ~8.2 nm for one division in PM fiber [b]: Corresponding pulse burst at Port M; the inset shows the autocorrelation of the externally amplified, recombined pulse at Port T with 0.8 ps duration. [c], [d]: Port T spectral bandwidth (8.3 nm FWHM) and pulse burst at Port M for two pulse divisions with additional 10 mm YVO_4-crystal, respectively. The recombined pulse at Port T (Inset [d]) has a FWHM of 0.83 ps. [e], [f]: Port T spectral bandwidth (8.2 nm FWHM) and Port M pulse burst autocorrelation for a third division with an additional 20 mm YVO_4-crystal. Inset [f]: Recombined and amplified pulse at Port T with 0.8 ps FWHM.

This unique cavity structure enables the application of a YVO_4-based DPA scheme as the intrinsic compensation of linear phase shifts enables the coherent recombination of divided pulses. For the setup in Fig.1 [a], the divider consists of a 10 mm and a 20 mm long YVO_4-crystal in series in combination with the birefringent PM fiber that causes a total delay of ~2.8 ps. The delay caused by the YVO_4 is ~0.8 ps/mm at 1030 nm due to the large material birefringence of B=0.208. The fast axis sequential rotation angles in the DPO pulse divider with respect to the transmission axis of PBS1 for the two YVO_4-crystals and the PM fiber are 45°, 0° and 45°, respectively. Fig.1 [b] shows the resulting shape of $T(\Delta\varphi_{nl})$ for different values of phase-bias settings derived through an implementation of the YVO_4-crystals into the model of Ref. [10] with the corresponding Jones-matrices for the birefringent elements. A simulation of the

pulse burst after the first 45°-rotated, 10 mm YVO_4-crystal can be seen in Fig.1 [c]. The phase-bias waveplate angles of θ=10° and ξ=25° ensure an energy splitting ratio of ε=0.8 with a positive slope of $T(\Delta\varphi_{nl})$ for small-signal values of $\Delta\varphi_{nl}$. Fig.1 [d] and [e] show the simulated divided pulses with two and three divisions after the subsequent, 0°-rotated 20 mm YVO_4-crystals and the PM-fiber segment at Port M, respectively. The pulse burst in Fig. 1 [d] that propagates through the PM-fiber segment consists of three identical copies of the fundamental asymmetric pulse pair with identical nonlinear propagation characteristics and accumulated nonlinear phase difference $\Delta\varphi_{nl}$.

In the fundamental mode-locked state, the oscillator generates soliton-like pulses with an output energy of 89 pJ measured at Port T with a QWP2 rotation angle that ensures an output coupling ratio of 30%. Fig.2 [a] shows the spectrum of the pulse with ~8.2 nm FWHM centered at 1038 nm. Fig.2 [b] shows the autocorrelation (AC) trace of the pulse burst measured at Port M with ~2.8 ps delay for the orthogonal polarization modes after a single-pass through the PM-fiber. Simultaneously, the AC trace of a single recombined pulse can be measured at Port T with a FWHM of 0.8 ps. The deviation from the transform limit is due to the required external amplification of the Port T and Port M pulse trains with an auxiliary fiber amplifier to ensure sufficient peak power for the AC measurement.

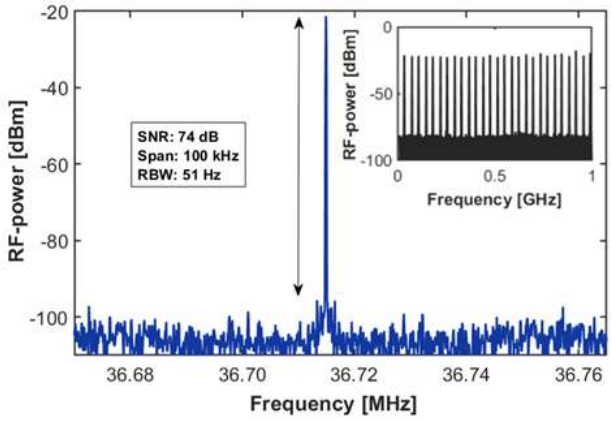

Fig. 3: RF-spectrum of the DPO fundamental repetition-rate with 3 divisions at 36.7 MHz measured over a span of 100 kHz with 51Hz RBW. The SNR is ~74 dBm. The inset shows higher harmonics over a 1 GHz span (RBW: 100 kHz).

In this state, the laser is self-starting at a pump power of ~300 mW. Single-pulse operation can be achieved by reducing the pump power to ~75 mW. The verification of stable single-pulse operation is based on multiple separate measurements. As a first step, the 150 ps wide-range autocorrelation together with a 0.02 nm high-resolution spectral measurement is used to ensure the absence of periodic modulations in the spectrum. Further, the pulse train at Port T is detected with a fast InGaAs PIN photodetector (EOT-3000) and the radiofrequency (RF)-spectrum is measured with a spectrum analyzer (Keysight N9000A) over the full photodetector bandwidth of 2 GHz (100 kHz resolution) to verify the absence of amplitude-modulations of the higher harmonics. Fig.2 [c] shows the optical spectrum at Port T with a second pulse divider in the cavity. Here, the polarization modes are first separated in the 45°-rotated, 10mm YVO_4-crystal with a delay of ~8 ps and then further divided in the 0°-rotated PM-fiber segment. The corresponding autocorrelation of the pulse burst measured at Port M is shown in Fig.2[d] together with the autocorrelation trace of the recombined pulse at Port T with a FWHM of 0.83 ps and a pulse energy of ~190 pJ. Subtle spectral modulations in conjunction with small perturbations in the AC-trace indicate a distorted recombination of the pulse burst e.g., due to deviations from ideal divider rotation angles and tolerances of the Faraday-mirror. The observed changes of the Kelly sidebands can be explained with a shifting cavity dispersion due to the additionally implemented YVO_4-crystals, a shifting working point on $T(\Delta\varphi_{nl})$ in steady-state and slightly different gain dynamics due to the higher intracavity power. Self-starting operation requires a ~700 mW pump power while the single-pulse threshold is at ~160 mW. The higher pump power for self-starting operation is required for an accumulation of sufficient small signal $\Delta\varphi_{nl}$ despite the reduced peak power due to the pulse division. For the third division, the 20mm YVO_4-crystal is implemented in the cavity with a 0°-rotation angle between the 45°-rotated 10 mm crystal and the 45°-rotated fiber.

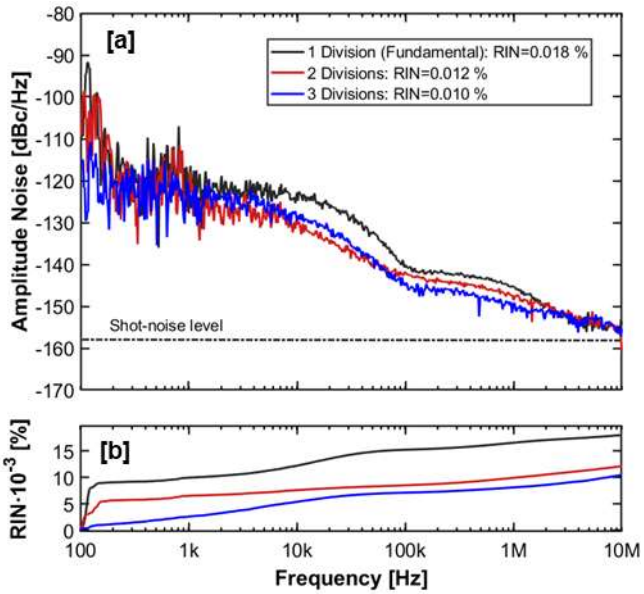

Fig. 4: [a]: Frequency-resolved AM noise spectra measured at Port T with different pulse divisions in the cavity. [b]: Corresponding RIN integrated from 100 Hz to 10 MHz for the fundamental state, 2 divisions and 3 division with RIN values of 0.018%, 0.012% and 0.010%, respectively.

The resulting spectral bandwidth (8.2 nm FWHM) together with the corresponding autocorrelations of the pulse burst at Port M and that of the recombined pulse at Port T (0.8 ps FWHM) can be seen in Fig.2 [e] and [f], respectively. For this state, the output pulse energy is increased by 6.5 dB to 400 pJ compared to the fundamental operation. Starting the laser in this state requires a pump power of up to 1.5 W with the single-pulse threshold at 400 mW. Further divisions were not possible in the experiment due to the lack of available pump power for initiation of mode-locking.

A significant aspect for the analysis of the DPO characteristics is the influence of each consecutive pulse division on the overall cavity stability and noise performance. Fig.3 shows the RF-spectrum of the

fundamental frequency of 36.7 MHz measured at Port T with 3 pulse divisions corresponding to the working point shown in Fig.2 [e] and [f]. The signal-to-noise ratio (SNR) is ~74 dBm with a span of 100 kHz and a resolution bandwidth (RBW) of 51 Hz. The inset of Fig.3 shows the broadband RF-spectrum with a span of 1 GHz measured with a RBW of 100 kHz. Furthermore, the amplitude-noise (AM-noise) of the recombined pulse train emitted at Port T for different division states of the oscillator is measured with the method described in Ref. [27]. Once the optical pulse train is converted to the electrical RF-domain with a fast photodetector (EOT-3000), the 5th harmonic at 183.5 MHz of the received RF-signal is filtered with a tunable bandpass filter and amplified with a 10dB trans-impedance amplifier to an RF-power of -1 dBm which is kept consistent for all measurements. The AM-noise function of the signal-source analyzer (SSA, Keysight E5052B) is used to measure the single-sideband noise spectral density. Experimental results of the AM-noise measurements at Port T in the range from 100 Hz to 20 MHz are shown in Fig.4 [a] for a different number of pulse divisions. In the high-frequency range from 100 kHz to ~3 MHz the AM-noise is significantly reduced (by up to 3 dB) with 2 pulse divisions in the cavity and by up to 6dB with 3 divisions, most likely because of the increased intracavity power as proposed in Ref. [18]. The AM-noise reduction is also present in the mid frequency-range from 10 kHz to 100 kHz by up to 9dB with the 10 mm crystal in the YVO_4-divider and up to 7 dB for the third division with the additional 20 mm crystal. Fig.4 [b] shows the corresponding relative intensity noise (RIN) integrated from 100 Hz to 20 MHz, excluding the influence of the technical noise sources <100Hz. For the fundamental mode-locked state, the RIN has a value of 0.018% that is consecutively reduced to 0.012% and 0.010% for the second and third division, respectively. The observable AM-noise variation for higher divisions can be explained through the averaging character of the coherent recombination. It is further influenced by the interplay between a shifting operation point away from the lasing threshold for more divisions, resulting in an increased stability as shown in Ref. [28] and occurring changes of the Port T noise-transfer due to a shifting working point on $T(\Delta\varphi_{nl})$ [12].

In conclusion, an all-PM Kerr-type fiber oscillator is investigated that uses periodic pulse division and recombination to reduce excessive roundtrip nonlinear phase shifts. The implementation of birefringent pulse division is enabled due to the linear cavity structure with intrinsic compensation of linear phase shifts based on a Faraday-mirror. In the experiment, the output pulse energy is increased by 6.5 dB from 89 pJ in the fundamental state to more than 400 pJ with 3 divisions. The stability of the mode-locked DPO for different divisions is investigated based on RF-characteristics and the AM-noise of the output pulse train. The measured AM-noise is found to be reduced by up to 6dB in the high offset-frequency range from 100 kHz to 3 MHz. The increased pulse energy in conjunction with significantly improved noise performance of the DPO is another step towards ultra-low noise fiber laser systems.

Funding. Deutsche Forschungsgemeinschaft (KA 908/9-1MUJO), European Research Council (609920).

Disclosures. The authors declare no conflicts of interest.

Data availability. Data underlying the results presented in this paper are not publicly available at this time but may be obtained from the authors upon reasonable request.

References

1. B. R. Washburn, S. A. Diddams, N. R. Newbury, J. W. Nicholson, M. F. Yan, and C. G. Jørgensen, Opt. Lett. **29**, 250-252 (2004).
2. M. Müller, C. Aleshire, A. Klenke, E. Haddad, F. Légaré, A. Tünnermann, and J. Limpert, Opt. Lett. **45**, 3083-3086 (2020)
3. M. Xin, K. Şafak, M. Peng, A. Kalaydzhyan, W. Wang, O.D. Mücke, and F. X. Kärtner, Light Sci Appl **6**, e16187 (2017).
4. R. Bouchand, X. Xie, D. Nicolodi, M. Giunta, W. Hänsel, M. Lezius, A. Joshi, S. Datta, C. Alexandre, M. Lours, P. Tremblin, G. Santarelli, R. Holzwarth, and Y. Coq, IEEE Phot. Tech. Lett. **29**, 1403-1406 (2017).
5. C.-J. Chen, P. K. A. Wai, and C. R. Menyuk, Opt. Lett. **20**, 350-352 (1995).
6. V. J. Matsas, D. J. Richardson, T. P. Newson, and D. N. Payne, Opt. Lett. **18**, 358-360 (1993).
7. L. A. Gomes, L. Orsila, T. Jouhti and O. G. Okhotnikov, IEEE J. Sel. Top. Quantum Electron. 10, 129-136 (2004).
8. J. Szczepanek, T. M. Kardaś, M. Michalska, C. Radzewicz, and Y. Stepanenko, Opt. Lett. **40**, 3500-3503 (2015).
9. D. Kim, D. Kwon, B. Lee, and J. Kim, Opt. Lett. **44**, 1068-1071 (2019).
10. A. S. Mayer, W. Grosinger, J. Fellinger, G. Winkler, L. W. Perner, S. Droste, S. H. Salman, C. Li, C. M. Heyl, I. Hartl, and O. H. Heckl, Opt. Express **28**, 18946-18968 (2020)
11. Y. Ma, S. H. Salman, C. Mahnke, Y. Hua, S. Droste, J. Fellinger, A. S. Mayer, O. H. Heckl, C. M. Heyl and I. Hartl, J. Lightwave Technol. **39**, 4431-4438 (2021).
12. M. Edelmann, Y. Hua, K. Şafak, and F. X. Kärtner, Opt. Lett. **46**, 1752-1755 (2021).
13. W. Hänsel, H. Hoogland, M. Giunta, S. Schmid, T. Steinmetz, R. Doubek, P. Mayer, S. Dobner, C. Cleff, M. Fischer, and R. Holzwarth, Appl. Phys. B Lasers Opt. **123**, 41 (2017).
14. N. Nishizawa, H. Suga, and M. Yamanaka, Opt. Express **27**, 19218-19232 (2019).
15. M. E. Fermann, L.-M. Yang, M. L. Stock, and M. J. Andrejco, Opt. Lett. 19, 43-45 (1994).
16. R. S. Fodil, F. Amrani, C. Yang, A. Kellou, P. Grelu, Phys. Rev. A **94**, 013813 (2016).
17. J. Peng, L. Zhan, S. Luo, and Q. Shen, J. Lightwave Technol. **31**, 3009-3014 (2013).
18. R. Paschotta, Opt. Express **18**, 5041-5054 (2010).
19. R. Paschotta, Appl. Phys. B **79**, 163-173 (2004).
20. H. A. Haus and A. Mecozzi. "Noise of mode-locked lasers." IEEE J. of Quant. Electron. **29**, 983-996 (1993).
21. W. Liu, H. Shi, J. Cui, C. Xie, Y. Song, C. Wang, and M. Hu, Opt. Lett. **43**, 2848-2851 (2018).
22. J. W. Nicholson and M. Andrejco, Opt. Express 14, 8160-8167 (2006)
23. A. Chong, J. Buckley, W. Renninger, and F. Wise, Opt. Express **14**, 10095-10100 (2006).
24. E. S. Lamb, L. G. Wright, and F. W. Wise, Opt. Lett. **39**, 2775-2777 (2014).
25. S. Zhou, F. W. Wise, and D. G. Ouzounov, Opt. Lett. **32**, 871-873 (2007).
26. M. Müller, C. Aleshire, A. Klenke, E. Haddad, F. Légaré, A. Tünnermann, and J. Limpert, Opt. Lett. **45**, 3083-3086 (2020).
27. M. Edelmann, Y. Hua, K. Şafak, and F. X. Kärtner, Opt. Lett. **46**, 3344-3347 (2021).
28. L. Matos, O. D. Mücke, J. Chen, and F. X. Kärtner, Opt. Express 14, 2497-2511 (2006)